



EXPERIMENTAL VERIFICATION OF VARIABLE-STIFFNESS ISOLATORS WITH DOUBLE CONCAVE SLIDING SURFACES

Lyan-Ywan Lu ⁽¹⁾, Yang Wu ⁽²⁾, Han-Wei Huang ⁽³⁾, Shao-Jou Wang ⁽⁴⁾

⁽¹⁾ Professor, National Cheng Kung University, Tainan, Taiwan, lylu@mail.ncku.edu.tw

⁽²⁾ Master of Science, National Cheng Kung University, Tainan, Taiwan, wuyang1654855734@gmail.com

⁽³⁾ Master of Science, National Cheng Kung University, Tainan, Taiwan, liggl159@gmail.com

⁽⁴⁾ Graduate Assistant, National Cheng Kung University, Tainan, Taiwan, sophia55103@gmail.com

Abstract

An isolation system with traditional sliding bearings, such as friction pendulum isolators (FPIs), is usually a long-period system with constant isolation frequency. Although this type of isolation systems may perform well in a far-field earthquake, its seismic response is likely to be amplified in a near-fault earthquake with long-period components. In order to enhance isolation performance and prevent excessive isolator displacement due to near-fault earthquakes, in this study, a new type of passive adaptive sliding isolators named the double sliding isolator with variable curvature (DSIVC) is studied experimentally. A DSIVC isolator mainly consists of an upper and a lower variable-curvature sliding interfaces and a slider placed in between the two sliding interfaces. The isolator stiffness provided by a DSIVC will vary along with the isolator displacement. Therefore, compared with an FPI, the DSIVC possesses adaptive nature that helps avert the resonant-like response exerted by a near-fault earthquake and thus lead to a smaller isolator size. Moreover, since a DSIVC has two sliding interfaces, it is able to provide an equal isolator displacement capacity with a smaller isolator size, so both manufacture cost and installation space of the isolators can be reduced. The above features make the DSIVC a more economical and efficient isolator. In this paper, a bi-directional analytical model for a general DSIVC will be introduced and verified experimentally by conducting an element cyclic test with uni- and bi-directional excitations. The experimental and theoretical results of this study verify the feasibility and adaptability of the DSIVC isolation technology.

Keywords: variable sliding isolator, variable stiffness, adaptive isolator, variable curvature, double sliding surfaces.



1. Introduction

Traditional sliding isolators, e.g., friction pendulum isolators (FPIs), have been proved to be a very effective means for seismic protection of structures or equipment under a regular earthquake [1]. An FPI usually has a spherical sliding surface of constant curvature that results in a constant isolation stiffness and vibration period. Recent studies have discovered that an isolation system consisting of this type of isolators may incur excessive isolator displacement in a near-fault earthquake with long-period pulse components, due to a resonant-like response [2-3]. Consequently, in order to ensure the safety of an FPI-isolated structure located in a near-fault area, the design size of sliding bearings have be enlarged dramatically, and thus the manufacturing cost and installation space will be considerably increased as well.

To overcome this isolation problem associated with long-period earthquakes while to maintain the isolation efficiency in far-field (regular) earthquakes, which usually do not contain long-period components, some researchers have proposed using sliding isolators with variable curvature (SIVC), which have a concave and axially symmetric sliding surface with variable curvature [4-11]. As a result, the isolation stiffness and frequency of an SIVC isolation system will vary along with the isolator displacement. Compared with an FPI, the SIVC possesses adaptive nature that may help avert the resonant-like response under a near-fault earthquake and thus lead to a smaller isolator size, provided that the geometry of the sliding surface is properly designed. The effectiveness and feasibility of SIVCs has been verified both theoretically and experimentally in the previous works by the authors of the present paper [6, 7, 11].

To further reduce the dimension of SIVC isolators, the notion of double sliding isolators with variable curvature (DSIVCs) was proposed in recent literature but has not been verified by experiment [12, 13]. Different from a SIVC that has only one concave sliding surface, a typical DSIVC isolator mainly is composed of an upper and a lower variable-curvature sliding interfaces and a slider. The slider, with friction pads on its both sides, is placed in between the two sliding surfaces. A DSIVC is physically similar to a double friction pendulum isolator (DFPI), except that its dual sliding surfaces are not made spherical, but with variable curvature [14]. A DSIVC has all the advantages and features of the SIVC mentioned above. Moreover, since it has two sliding surfaces, the DSIVC is able to provide an equal isolator displacement capacity with a smaller isolator size, so both manufacture cost and installation space of the isolators can be reduced. The DSIVC can also provide more adaptability and design flexibility than an SIVC does. These features make the DSIVC a more economical and efficient isolator. The objective of this study is to derive the formula of bi-directional force-displacement relation for the DSIVC and to verify the formula experimentally by conducting a DSIVC element test. Through the analytical and experimental study, it is expected that the outcome of this paper will expertise the application of sliding-type passive adaptive isolation systems.

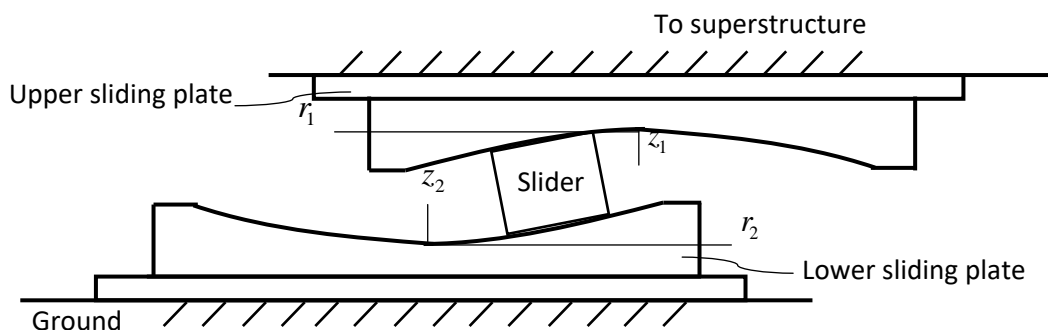


Fig. 1 – Schematic diagram of a double sliding isolator with variable curvature (DSIVC)



2. Formulation of bi-directional force-displacement relation for a DSIVC

2.1 Mathematical model

Figure 1 shows the schematic diagram of a DSIVC isolator that consists of an upper sliding plate, a lower sliding plate and a slider placed between the sliding plates. Similar to those of a DFPI isolator, the sliding surfaces of the upper and lower plates of the DSIVC are symmetrical about their central axes (i.e., z_1 and z_2 axes in Fig. 1), but their curvature is variable along with the radial coordinates r_1 and r_2 (see Fig. 1). Consequently, the geometric shapes of the upper and lower sliding surfaces can be defined by the geometric functions (or the elevation functions) $z_1(r_1)$ and $z_2(r_2)$. The slider that is in contact with both sliding surfaces has a friction pad on each of its two sides. The isolator friction force will be determined by the material property of the friction pads. Since the DSIVC has two sliding surfaces, it is able to provide displacement capacity equal to that of an SIVC but with an isolator size about one-half of the DSIVC size.

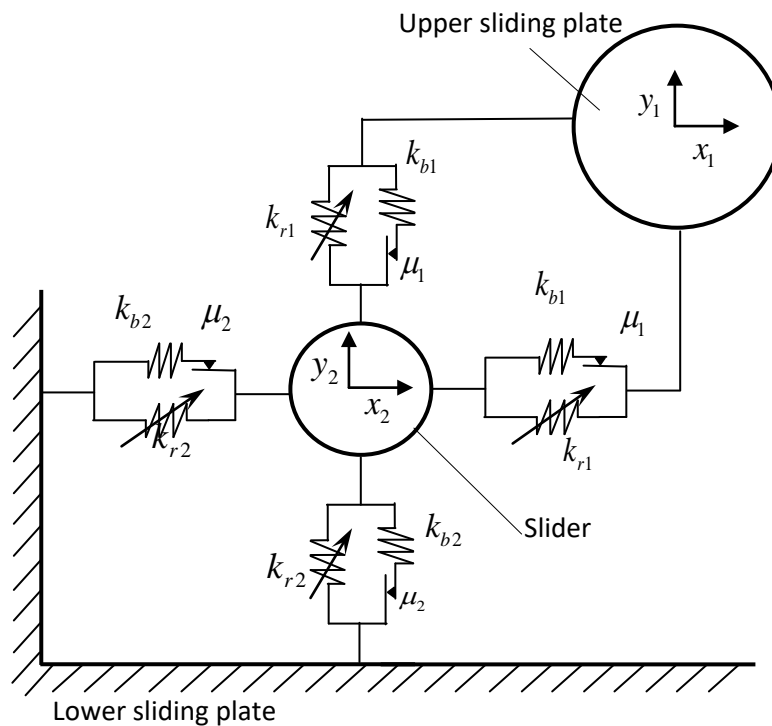


Fig. 2 – Mathematical model of a DSIVC

The mathematical model for the DSIVC under bi-directional motion may be depicted by Fig. 2. In the figure, x_1 and y_1 are the displacements of the upper sliding plate relative to the slider in x and y directions, respectively, while x_2 and y_2 are the slider displacements relative to the lower sliding plate in x and y directions, respectively. Symbols μ_1 and μ_2 represent the friction coefficients between the slider and upper and lower sliding plates. Symbols k_{b1} and k_{b2} may denote the stiffness of the upper and lower sliding plates. In latter numerical simulation, k_{b1} and k_{b2} will be assigned a very large value for numerical stability. Moreover, symbols k_{r1} and k_{r2} represent the effective isolation stiffness generated by the concaved upper and lower sliding surfaces, respectively. The values of k_{r1} and k_{r2} will depend on the chosen geometric functions of the upper and lower sliding surfaces, and can be expressed as

$$k_{r1}(r_1) = \frac{W z_1'(r_1)}{r_1}, \quad k_{r2}(r_2) = \frac{W z_2'(r_2)}{r_2} \quad (1)$$

where



$$r_1 = \sqrt{x_1^2 + y_1^2}, \quad r_2 = \sqrt{x_2^2 + y_2^2} \quad (2)$$

In Eq. (1), W denotes the axial load of the DSIVC isolator, and $z_1'(r_1)$ denotes the first derivative of $z_1(r_1)$ with respect to r_1 .

2.2 Derivation of force-displacement relation

In order to obtain a unique solution for the force-displacement relation for the DSIVC, the following three conditions of mechanics have to be satisfied simultaneously: equilibrium condition, element constitutive law and geometric compatibility condition. These mechanical conditions will be established in this subsection by using Fig. 2.

(1) Bi-directional equilibrium condition:

As shown Fig. 1 and Fig. 2, since the upper and lower sliding plates are placed in series, the shear forces between the slider and two sliding surfaces should be equal, i.e.,

$$U_{1x} = U_{2x}, \quad U_{1y} = U_{2y} \quad (3)$$

where U_{1x} and U_{2x} denote the x-directional horizontal shear forces of the upper and lower sliding plates, respectively; while U_{1y} and U_{2y} denote the y-directional shear forces of the upper and lower plates, respectively. Eq. (3) can be further rewritten in the following matrix form

$$\mathbf{D}_0 \mathbf{U} = \mathbf{0} \quad (4)$$

where

$$\mathbf{U} = \begin{Bmatrix} U_{1x} \\ U_{1y} \\ U_{2x} \\ U_{2y} \end{Bmatrix}, \quad \mathbf{D}_0 = \begin{bmatrix} 1 & 0 & -1 & 0 \\ 0 & 1 & 0 & -1 \end{bmatrix} \quad (5)$$

Furthermore, the model shown in Fig. 2 indicate the isolator shear forces mentioned above actually involve frictional and restoring force components provided by the frictional element and the variable spring elements (k_{r1} and k_{r2}), respectively; therefore, we have

$$\mathbf{U} = \mathbf{u}_r + \mathbf{u}_f \quad (6)$$

where \mathbf{u}_r and \mathbf{u}_f denote the vectors of the restoring force and frictional force, respectively, and can be written explicitly as

$$\mathbf{u}_r = \begin{Bmatrix} \mathbf{u}_{r1} \\ \mathbf{u}_{r2} \end{Bmatrix} = \begin{Bmatrix} u_{r1x} \\ u_{r1y} \\ u_{r2x} \\ u_{r2y} \end{Bmatrix}, \quad \mathbf{u}_f = \begin{Bmatrix} \mathbf{u}_{f1} \\ \mathbf{u}_{f2} \end{Bmatrix} = \begin{Bmatrix} u_{f1x} \\ u_{f1y} \\ u_{f2x} \\ u_{f2y} \end{Bmatrix} \quad (7)$$

where u_{r1x} and u_{r1y} denote the restoring forces provided by the upper sliding plate in x and y directions, respectively; u_{r2x} and u_{r2y} are the restoring forces provided by the lower sliding plate in x and y directions, respectively; u_{f1x} and u_{f1y} denote the frictional forces exerted on the upper sliding surface; u_{f2x} and u_{f2y} denote the frictional forces exerted on the lower sliding surface.



(2) Element constitutive law:

Fig. 2 indicates that the restoring forces of the DSIVC in each direction shall depend on the variable stiffness (k_{r1} and k_{r2}) and isolator displacements in that direction; therefore, the restoring forces can be expressed as

$$\mathbf{u}_r = \mathbf{K}_r \mathbf{X}_r \quad (8)$$

where

$$\mathbf{K}_r = \begin{bmatrix} k_{r1} & 0 & 0 & 0 \\ 0 & k_{r1} & 0 & 0 \\ 0 & 0 & k_{r2} & 0 \\ 0 & 0 & 0 & k_{r2} \end{bmatrix}, \quad \mathbf{X}_r = \begin{Bmatrix} x_1 \\ y_1 \\ x_2 \\ y_2 \end{Bmatrix} \quad (9)$$

In the last equation, \mathbf{K}_r is the stiffness matrix, \mathbf{X}_r denotes the displacement vector containing bi-directional displacements of the upper and lower sliding plates, isolation stiffness k_{r1} and k_{r2} have been defined in Eq. (1). Eq. (8) is also known as the element constitutive law for the DSIVC. Further substituting Eq. (8) in Eq. (6) yields

$$\mathbf{U} = \mathbf{K}_r \mathbf{X}_r + \mathbf{u}_f \quad (10)$$

Also, substituting Eq. (10) in Eq. (4), one may rewrite the equilibrium equation as following

$$\mathbf{D}_0 \mathbf{K}_r \mathbf{X}_r + \mathbf{D}_0 \mathbf{u}_f = \mathbf{0} \quad (11)$$

(3) Geometric compatibility condition:

In view of Fig. 1 and Fig. 2, the upper and lower sliding plates are placed in series, so the total isolator displacement of the DSIVC in a certain direction should be equal to the addition of the displacements of the upper and lower sliding plates in that direction. Therefore, we have

$$\mathbf{D}_1 \mathbf{X}_r = \mathbf{X}_t \quad (12)$$

where

$$\mathbf{D}_1 = \begin{bmatrix} 1 & 0 & 1 & 0 \\ 0 & 1 & 0 & 1 \end{bmatrix}, \quad \mathbf{X}_t = \begin{Bmatrix} x_t \\ y_t \end{Bmatrix} \quad (13)$$

where symbols x_t and y_t represent the isolator total displacement in the x and y directions, respectively.

(4) Bi-directional force-displacement relation for DSIVC:

Next, combining Eq. (11) (the equilibrium condition) and Eq. (13) (the compatibility condition) yields

$$\mathbf{K}(t) \mathbf{X}_r(t) = \hat{\mathbf{B}} \mathbf{u}_f(t) + \hat{\mathbf{E}} \mathbf{X}_t(t) \quad (14)$$

where

$$\mathbf{K}(t) = \begin{bmatrix} \mathbf{D}_0 \mathbf{K}_r(t) \\ \mathbf{D}_1 \end{bmatrix}, \quad \hat{\mathbf{B}} = \begin{bmatrix} -\mathbf{D}_0 \\ 0 \end{bmatrix}, \quad \hat{\mathbf{E}} = \begin{bmatrix} 0 & 0 \\ 0 & 0 \\ 1 & 0 \\ 0 & 1 \end{bmatrix} \quad (15)$$



Finally, solving Eq. (14) for vector \mathbf{X}_r and substituting the solution into Eq. (10), we have

$$\mathbf{U}(t) = (\mathbf{K}_r(t)\mathbf{B}(t) + \mathbf{I})\mathbf{u}_f(t) + \mathbf{K}_r(t)\mathbf{E}(t)\mathbf{X}_t(t) \quad (16)$$

where

$$\mathbf{B}(t) = \mathbf{K}^{-1}(t)\hat{\mathbf{B}}, \quad \mathbf{E}(t) = \mathbf{K}^{-1}(t)\hat{\mathbf{E}} \quad (17)$$

Eq. (16) describes the bi-directional relationship between the isolator's internal shear forces $\mathbf{U}(t)$ and total displacements $\mathbf{X}_t(t)$ for a DSIVC. This equation will be used to compute the isolator shear forces and to generate the numerical hysteresis loop of the DSIVC, which will be compared with the test results.

3. Element cyclic test of DSIVC

3.1 Description of specimen – DPFPI isolator

In order to verify the feasibility of DSIVC isolation technology and the correctness of the force-displacement formula derived in the previous section, an element cyclic test was conducted for a DSIVC isolator. The geometric functions for the upper and lower sliding surfaces of the tested DSIVC are identical. The following 8th order polynomial function, which is similar to the one proposed by Lu et al. [6] for a SIVC, was adopted as the geometric function for both sliding surfaces.

$$z(r) = \frac{a_1}{8}r^8 + \frac{b_1}{6}r^6 + \frac{c_1}{4}r^4 + \frac{d_1}{2}r^2 \quad (18)$$

where a_1 , b_1 , c_1 and d_1 are constant coefficients, and r is the radial coordinate (see Fig. 1). Since the geometric function of the tested DSIVC is defined by the polynomial of Eq. (18), hereafter the tested specimen is called the double polynomial friction pendulum isolator (DPFPI). Moreover, the polynomial coefficients in Eq. (18) are purely mathematic without engineering meaning. In this study, these coefficients will be converted into some design parameters for the convenience of design purpose, as will be explained below.

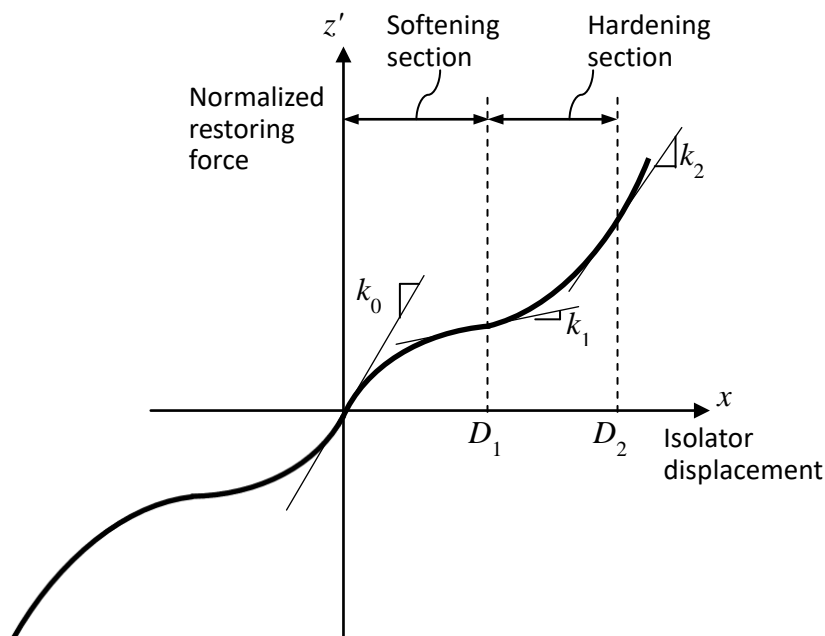


Fig. 3 – Normalized restoring force of the DPFPI



In the theory of SIVC with a single sliding surface, the first derivative $z'(r)$ of the geometric function is equivalent to the restoring force normalized with respect to the isolator's axial load W [6, 7]. Fig. 3 shows the curve of the normalized restoring force $z'(r)$ for one single sliding surface of the tested DPFPI, whose geometric function is defined by Eq. (18). As shown in Fig. 3, the normalized restoring force of the DPFPI possesses a softening section followed by a hardening section. Notably, five design parameters (k_0, k_1, k_2, D_1, D_2) are shown in Fig. 3. Among them, k_0 denotes the initial isolator stiffness; D_1 and D_2 are the isolator displacements corresponding two level design earthquakes usually specified in a seismic design code (e.g., DBE and MCE); k_1 and k_2 are the tangential stiffness at the displacements D_1 and D_2 , respectively. Note that D_1 is also the critical isolator displacement at which the isolator is changing from softening behavior to hardening behavior as shown in Fig. 3. With the above definition for the five design parameter, the relation between the four polynomial coefficients (a_1, b_1, c_1, d_1) and design parameters can be expressed by the following equations

$$a_1 = a_1(k_0, k_1, k_2, D_1, D_2) = \frac{D_1^4(k_0 - k_2) + D_2^2(k_0 - k_1)(D_2^2 - 2D_1^2)}{-7D_1^4D_2^2(D_1^2 - D_2^2)^2} \quad (19)$$

$$b_1 = b_1(k_0, k_1, k_2, D_1, D_2) = \frac{2D_1^6(k_0 - k_2) + D_2^2(k_0 - k_1)(D_2^4 - 3D_1^4)}{5D_1^4D_2^2(D_1^2 - D_2^2)^2} \quad (20)$$

$$c_1 = c_1(k_0, k_1, k_2, D_1, D_2) = \frac{D_1^6(k_0 - k_2) + D_2^4(k_0 - k_1)(2D_2^2 - 3D_1^2)}{-3D_1^2D_2^2(D_1^2 - D_2^2)^2} \quad (21)$$

$$d_1 = k_0 \quad (22)$$

Table 1 – Parameters of DPFPI sliding surfaces used in element test.

Parameter for single sliding surface				Equivalent parameter for double sliding surfaces	
Design parameter		Polynomial coeff.		Equivalent design parameter	
k_0	1.786 (1/m)	a_1	-432.505	$k_{e0} (= k_0 / 2)$	0.893 (1/m)
k_1	0.447 (1/m)	b_1	248.984	$k_{e1} (= k_1 / 2)$	0.223 (1/m)
k_2	2.233 (1/m)	c_1	-19.25	$k_{e2} (= k_2 / 2)$	1.116 (1/m)
D_1	0.080 (m)	d_1	0.8925	$D_{1,t} (= 2D_1)$	0.160 (m)
D_2	0.120 (m)	e_1	0.0	$D_{2,t} (= 2D_2)$	0.240 (m)

For the tested DPFPI, Table 1 lists the values of the five design parameters (k_0, k_1, k_2, D_1, D_2) and the corresponding four polynomial coefficients used to define dual sliding surfaces. Also listed in Table 1 are the equivalent design parameters ($k_{e0}, k_{e1}, k_{e2}, D_{1,t}, D_{2,t}$), which were obtained by treating the DPFPI as an equivalent isolator of single sliding layer. Notably, since the upper and lower sliding surfaces are identical, the values of the equivalent stiffness (k_{e0}, k_{e1}, k_{e2}) are exactly one half of those values for a single sliding surface, while the isolator design displacements ($D_{1,t}, D_{2,t}$) become twice of the values for a single sliding surface. For comparison purpose, in Fig. 4, the geometric function of one single sliding surface of the DPFPI is compared with that of a counterpart DFPI. The DFPI has two identical spherical sliding surfaces whose radius of curvature is 735 mm, which results in an effective pendulum period of 2.43s. Fig. 5 compares the



effective restoring forces (normalized with respect to the axial load W) of the DPFPI and the DFPI. Notably, Fig. 5 shows that the line of the DFPI intersects the curve of the DPFPI at the critical displacement $D_{1,t} = 0.16$ mm, and the DPFPI exhibits obvious hardening behavior when the isolator displacement goes beyond 200 mm.

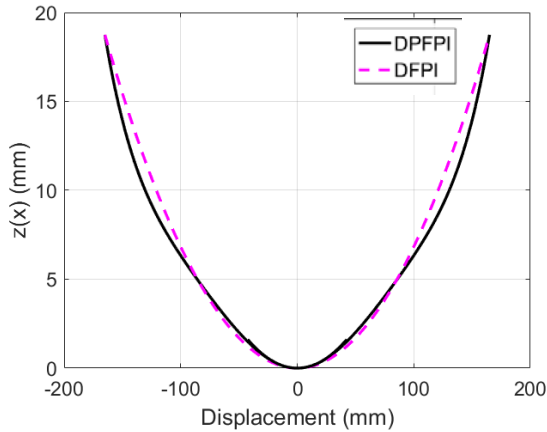


Fig. 4 – Geometric function of one single sliding surface of DPFPI and DFPI

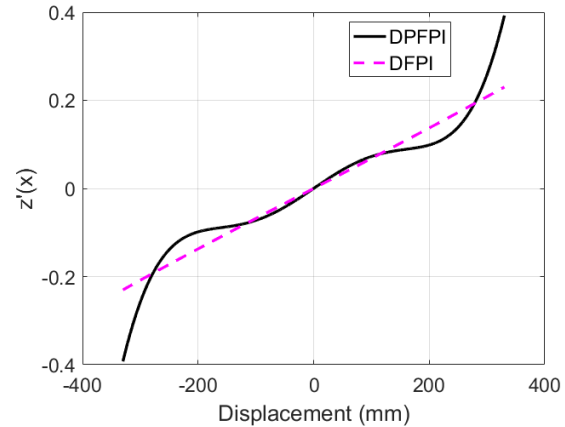


Fig. 5 – Normalized equivalent restoring forces of DPFPI and DFPI

Table 2 –Property of slider and friction pads for DPFPI.

Item	Parameter
Slider shape	Cylindrical
Slider height	40 mm
Friction pad diameter	50 mm
Friction coefficient	$\mu_f = 0.09, \mu_s = 0.05, \beta = 10$
Allowable isolator displacement	280 mm

Table 2 lists the properties of the slider and the friction pads. As shown in the table, the cylindrical slider has a height of 40 mm, and the diameter of the friction pads placed on both sides of the slider is 50 mm. The following Constantinou's friction model [15] was considered in the test and later numerical simulation,

$$\mu = \mu_f - (\mu_f - \mu_s) e^{-\beta|V|} \quad (23)$$

where μ_f and μ_s are the friction coefficients at high and low speed, respectively, V is sliding velocity and β is speed rate factor. Through the test data, these coefficients were identified to be $\mu_f = 0.09$, $\mu_s = 0.05$, $\beta = 10$.

3.2 Test setup and loading pattern

The element test of the DPFPI was conducted by using a hydraulic testing frame called Multi-axial Testing System (MATS) located in the Taipei laboratory of National Center for Research on Earthquake Engineering (NCREE). The MATS is designated for testing the bi-directional hysteretic properties of small-scale seismic isolators. Fig. 6 shows the local view of the test setup with a DPFPI. As shown, the isolator was placed on the moving platform of the MATS that is able to generate bi-directional horizontal motion, and a triaxial load cell (200 kN) was placed between the isolator and the vertical actuator to measure the vertical load and bi-



directional horizontal shear forces of the isolator. An optical sensing system made by NDI Inc. was employed to measure the 3D displacements of the DPFPI.

Two types of displacement excitations were imposed to the DPFPI in the test, namely, unidirectional and bi-directional excitations. In the unidirectional test, a sinusoidal excitation of frequency 0.05 Hz was applied on the DPFPI, while the displacement amplitude was increased in 3 steps (80, 160, 240 mm) (see Fig. 7(a)). In the bi-directional test, sinusoidal excitations were applied on the DPFPI in both x- and y-directions simultaneously with the loading frequencies of 0.1 Hz and 0.05 Hz, respectively. The displacement amplitudes in both directions were also increased in 3 steps (64, 128, 192 mm). The difference of loading frequencies in x- and y-directions creates an orbit of 8-shaped horizontal displacement on the tested DPFPI (see Fig. 8(a)). In all tests, the target vertical load was set to 40 kN. However, due to the elevation change of the sliding surface, variation on the vertical load was observed when the sliding speed increased.

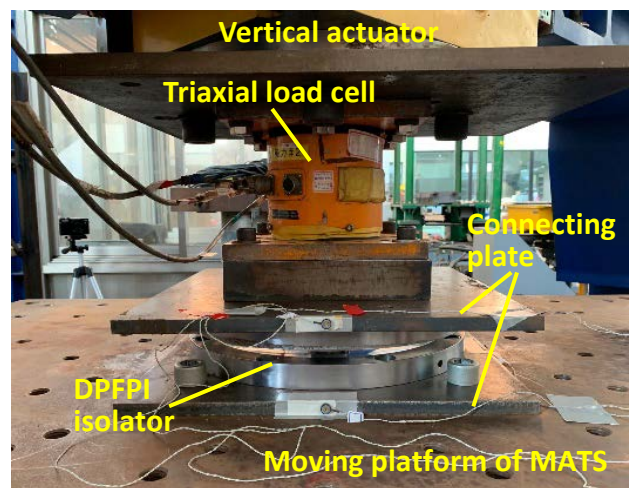


Fig. 6 – Setup of DPFPI element test

4. Comparison of experimental and theoretical results

4.1 Result of unidirectional excitation test

Fig. 7 compares the experimental and simulated responses of the DPFPI under the unidirectional sinusoidal excitation. The subplots in Fig. 7 are (a) total isolator displacement, (b) isolator shear force, (c) isolator hysteresis loop, (d) slider displacements relative to the upper and lower sliding plate. Fig. 7(a) shows that the displacement generated by the MATS was able to exactly follow the given command. Fig. 7(b) shows that the experimental and simulated isolator shear forces match fairly well, except that the theoretical result underestimates the shear force in the larger displacement. Notably, in the numerical simulation of Fig. 7, k_{b1} and k_{b2} were taken to be 5.34×10^3 kN/m. From Fig. 7(c), it is observed that the experimental hysteresis loop exhibits softening behavior followed by hardening behavior, as predicted by the theoretical result. This demonstrates that the DPFPI is able to possess variable mechanical property. Fig. 7(d) shows that the slider displacements relative to the upper and the lower sliding plates are equal and consistent, as expected by the theory. Nevertheless, there is a relatively large discrepancy between the experimental and simulated results in the hysteresis loop of Fig. 7(c) under the largest amplitude. This inconsistency may be due to the dimension (size) effect of the slider. Since the general formula derived in the previous section for a DSIVC assumes that the slider is a particle that can only exert point loads. However, in reality there is a contact area between the slider and the sliding surfaces. Consequently, the isolator stiffness predicted by Eq. (1) may produce modeling error.



4.1 Result of bi-directional excitation test

Fig. 8 compares the experimental and simulated responses of the DPFPI under the bi-directional sinusoidal excitation. In the figure, the subplots are (a) orbit of bi-directional isolator displacement, (b) shear force in x-direction, (c) shear force in y-direction, (d) hysteresis loop in x-direction, (e) hysteresis loop in y-direction. Fig. 8(a) shows that the MATS was able to follow the command and generated an 8-shaped bi-directional motion with a maximum radial displacement around 240mm. Figs. 8(b)-8(e) demonstrate that the theoretical results of the isolator shear forces and hysteresis loops in the both directions match well with the experimental results. This indicates that the formulation derived in the previous section is able to accurately predict the variable mechanical behavior of a DSIVC. The test results of Fig. 7 and Fig. 8 together also verify that the DSIVC is a feasibility isolation technology.

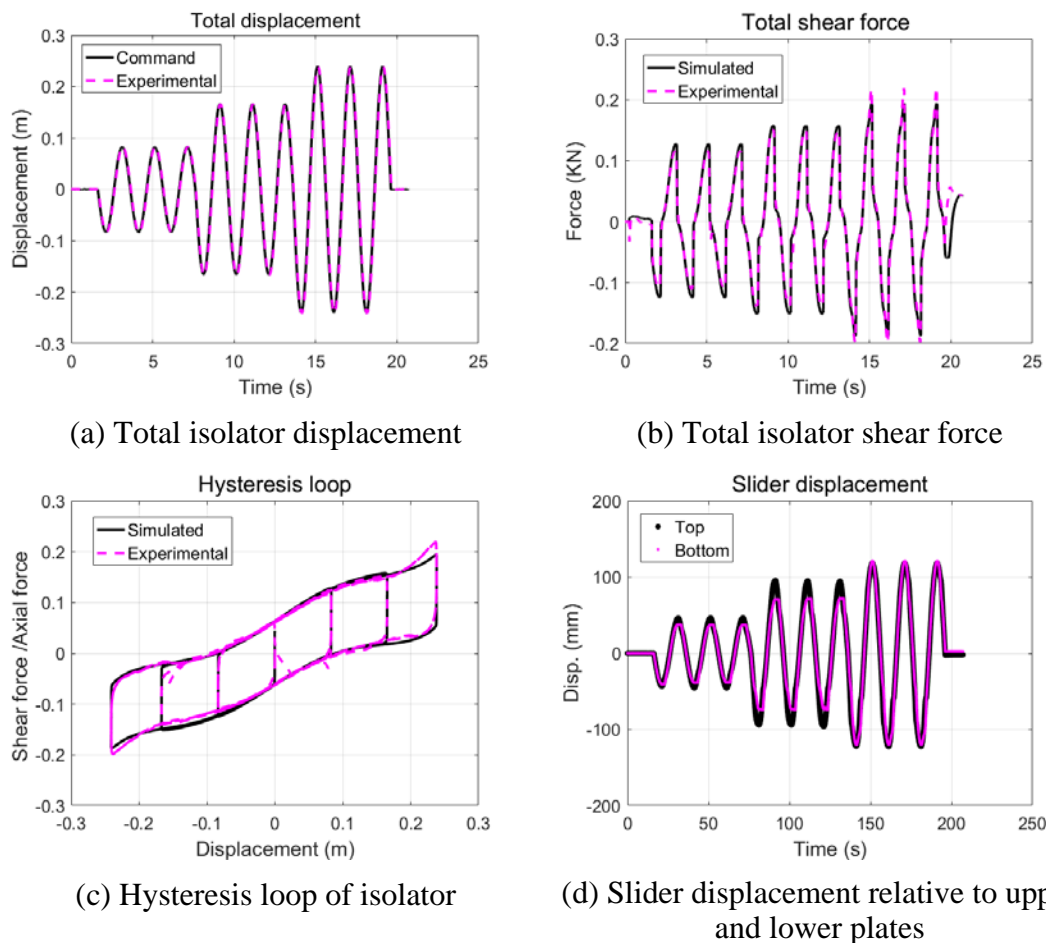


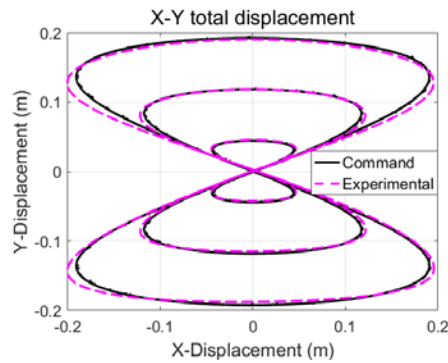
Fig. 7 – Comparison of experimental and simulated results of DPFPI under unidirectional sinusoidal excitation (Freq. = 0.05 Hz; axial load = 40 kN)

5. Conclusions

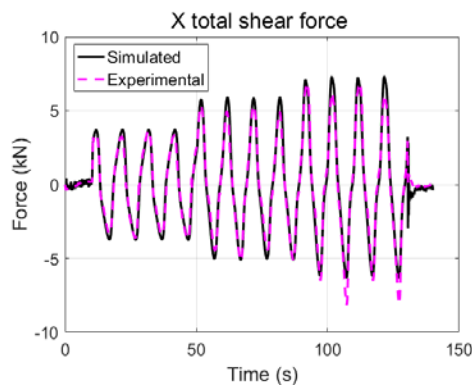
In order to enhance isolation performance of sliding-type seismic isolators, in this study, the feasibility of using a passive adaptive isolator called double sliding isolator with variable curvature (DSIVC) was studied theoretically and experimentally. Because a DSIVC isolator has double sliding surfaces with variable curvature, the DSIVC not only possesses all advantages of sliding-type isolators, but also exhibits adaptive nature and is more economical than traditional sliding isolators. In order to predict the mechanical behavior of the DSIVC, a formula describing bi-directional force-displacement relation of the DSIVC was first derived in this study, and then verified experimentally by a DSIVC element test. The formula was derived



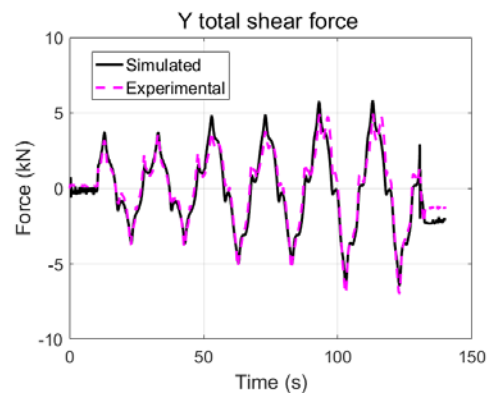
systematically by satisfying all mechanical conditions of the DSIVC, including equilibrium condition, constitutive law and geometric compatibility condition. The test result demonstrates that derived formula is able to predict the isolator shear force and hysteresis loop of the DSIVC under either unidirectional or bi-directional excitations. The experimental result also show that the DSIVC is able to exhibit adaptive nature with variable mechanical property, which can be prescribed by the geometric function of the double sliding surfaces. Therefore, the feasibility of DSIVC isolation technology is verified experimentally in this study.



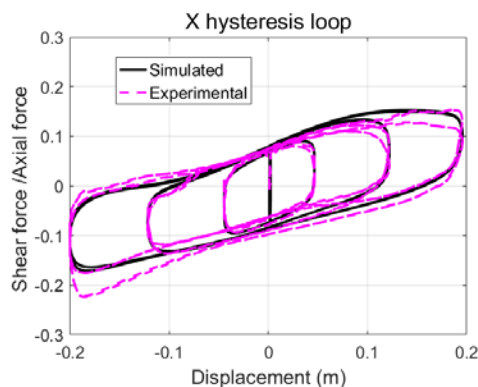
(a) Orbit of bi-directional displacement



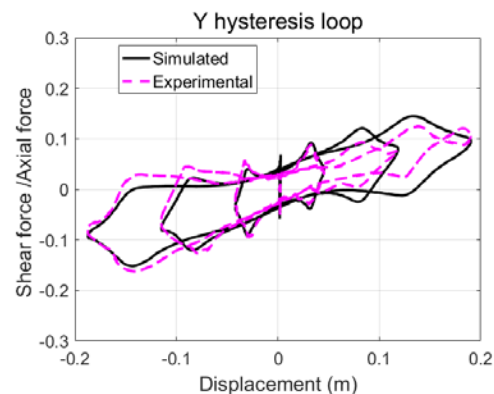
(b) X-dir. shear force



(c) Y-dir. shear force



(d) X-dir. hysteresis loop



(e) Y-dir. hysteresis loop

Fig. 8 – Comparison of experimental and simulated results of DPFP under bi-directional sinusoidal excitation (X-dir. freq. = 0.1 Hz; Y-dir. freq. = 0.05 Hz; axial load = 40 kN)



6. Acknowledgements

This research was supported in part by the Ministry of Science and Technology of R.O.C. (Taiwan) through grant MOST108-2625-M-006-005. The authors are grateful to the National Center for Research on Earthquake Engineering (NCREE, Taipei) for its technical support of the experiment.

7. References

- [1] Naeim F and Kelly JM (1999): *Design of Seismic Isolated Structures*. John Wiley & Sons, Inc., New York.
- [2] Zayas VA, Low SS (2000): Seismic Isolation for Strong Near-field Earthquake Motions. *The 12th World Conference on Earthquake Engineering*, Auckland, New Zealand, No.0088.
- [3] Lu LY, Lin CC, Lin GL (2013): Experimental evaluation of supplemental viscous damping for a sliding isolation system under pulse-like base excitation. *Journal of Sound and Vibration*, **332** (8), 1982-1999.
- [4] Murnal P and Sinha R (2002): Earthquake Resistant Design of Structures using the Variable Frequency Pendulum Isolator. *Journal of Structural Engineering*, **128**(7), 870-880.
- [5] Tsai CS, Chiang TC, Chen BJ (2003): Finite element formulations and theoretical study for variable curvature friction pendulum system. *Engineering Structures*, **25**, 1719-1730.
- [6] Lu LY, Lee TY, Yeh SW (2011): Theory and experimental study for sliding isolators with variable curvature. *Earthquake Engineering & Structural Dynamics*, **40**, 1609-1627.
- [7] Lu LY, Lee TY, Juang SY, Yeh SW (2013): Polynomial friction pendulum isolators (PFPIs) for building floor isolation: an experimental and theoretical study. *Engineering Structures*, **56**, 970-982.
- [8] Krishnamoorthy A (2015): Seismic control of continuous bridges using variable radius friction pendulum systems and viscous fluid dampers. *International Journal of Acoustics & Vibration*, **20**(1), 24-35.
- [9] Gidaris I, Taflanidis AA, Lopez-Garcia D, Mavroeidis GP (2016): Multi-objective risk-informed design of floor isolation systems. *Earthquake Engineering & Structural Dynamics*, **45**(8), 1293-1313.
- [10] Shaikhzadeh AA, Karamoddin A (2016): Effectiveness of sliding isolators with variable curvature in near-fault ground motions. *The Structural Design of Tall & Special Buildings*, **25**, 278-296.
- [11] Wang LW, Lu LY (2018): Generic 3D formulation for sliding isolators with variable curvature and its experimental verification. *Engineering Structures*, **177**, 12-29.
- [12] Panchal VR, Jangid RS, Soni DP, Mistry BB (2010): Response of the double variable frequency pendulum isolator under triaxial ground excitations. *Journal of Earthquake Engineering*, **14**, 527-558.
- [13] Soni DP, Mistry BB, Jangid RS, Panchal VR (2011): Seismic response of the double variable frequency pendulum isolator. *Structural Control & Health Monitoring*, **18**, 450-470.
- [14] Fenz DM and Constantinou MC (2006): Behaviour of the double concave friction pendulum bearing. *Earthquake Engineering and Structural Dynamics*, **35**, 1403-1424.
- [15] Constantinou MC, Mokha A, Reinhorn A (1990): Teflon bearings in base isolation II: modeling. *Journal of Structural Engineering, ASCE*, **116**, 455-74.